

https://doi.org/10.1070/QEL17607

Laser-plasma acceleration of polarised electrons up to energies of several TeV

D.V. Pugacheva, N.E. Andreev

Abstract. **The process of multistage acceleration of polarised electrons in the wakefield of a relativistic femtosecond laser pulse is investigated. The main mechanism of the growth of slice emittance for a moderately nonlinear regime of laser-plasma acceleration is demonstrated. The main conditions for setting the initial parameters of the electron bunch are determined, which allow minimising the mixing of the phases of betatron oscillations of particles in the bunch slice and the emittance growth during acceleration. The method of smooth input of an electron bunch into the accelerating stage and its smooth removal from this stage is studied, which allows the main characteristics of the bunch to be preserved, such as emittance and polarisation, for further particle transportation and acceleration. The effect of the radiation friction force and the radiation polarisation mechanism on the process of particle depolarisation in acceleration to energies of ∼4 TeV in model fields characteristic of moderately nonlinear and strongly nonlinear regimes of laser-plasma acceleration is considered.**

Keywords: *radiation polarisation, spin precession, laser-plasma acceleration, multistage acceleration, radiation dynamics.*

1. Introduction

Acceleration gradients achieved by laser-plasma acceleration methods are on the order of 100 GeV m^{-1} and significantly exceed those that can be obtained in radio frequency accelerators [1–4], which makes it possible to design compact charged particle accelerators based on these methods. Such accelerators can be widely used in science, medicine, and industry. For example, it is proposed to use a new type of accelerators in high-energy physics experiments, which require monoenergetic bunches of charged particles with an energy of several TeV, low emittance, and a prescribed spin polarisation [5]. One of the schemes of an electron–positron collider based on laser-plasma acceleration, which allows particles with similar characteristics to be obtained, involves combining about 100 separate accelerating stages with an energy gain of ∼10 GeV at each of them [6]. For other practical applications, such as the design of a free electron laser, the latest detector for experiments in high-energy physics or obtaining X-ray images with phase contrast, high-quality particle bunches with an energy of ∼5 GeV are also required [7–9]; therefore, the preservation of the initial bunch characteristics in the process of laser-plasma acceleration is an important problem.

The processes of injection of a bunch of particles into the accelerator and their removal are of particular complexity, since a nonadiabatic change in forces at the plasma boundary may lead to a significant increase in the bunch emittance [10, 11] and also affect the particle polarisation. The study of the depolarisation process is especially important for multistage acceleration of electrons to high energies, since the cross section of particle scattering in high-energy physics experiments depends on the orientation of the spins in the bunch [12, 13].

In laser-plasma acceleration with particle energies of several TeV, various effects associated with the betatron radiation of a particle may significantly contribute to the dynamics of the bunch characteristics [14–16]. In our work [15], we simulated electron acceleration in model fields characteristic of various regimes of laser-plasma acceleration, taking into account the classical radiation friction force in the Landau–Lifshitz form. The effect of the deceleration force on the energy gain and depolarisation during particle acceleration in a moderately nonlinear regime and the bubble regime was demonstrated.

During prolonged circulation of unpolarised electrons in the storage ring field, their spins, as a result of synchrotron radiation, are oriented in the direction opposite to the direction of the magnetic field. This effect of self-polarisation of relativistic charged particles during their long-term motion in a homogeneous constant magnetic field was first predicted by A.A. Sokolov and I.M. Ternov in 1963 [17] and its kinetics is determined by the characteristic polarisation time (in seconds) [18–20]

$$\tilde{T} = \frac{10^{-7}}{E_e^2 E_{acc}^3}, \tag{1}$$

where E_e is taken in GeV and E_{acc} is taken in TV m^{-1}. For electrons with energies E_e = 500 GeV – 2 TeV in an accelerating field E_{acc} = 100 GeV m^{-1}, the time determined by Eqn (1) lies in the range 400–25 ps, and the particle's interaction time with the field at acceleration from 500 MeV to 4 TeV is many times higher than these values and amounts to ∼13 μs; therefore, in the case of multistage acceleration, it is advisable to study not only the effect of the deceleration force on depolarisation, but also the contribution of radiation polarisation.

In this work, we study the mechanism of the growth of electron bunch emittance in a wakefield generated by a relativistic femtosecond laser pulse in a plasma channel in the

D.V. Pugacheva, N.E. Andreev Joint Institute for High Temperatures, Russian Academy of Sciences, ul. Izhorskaya 13, stroenie 2, 125412 Moscow, Russia; Moscow Institute of Physics and Technology (National Research University), Institutskiy per. 9, Dolgoprudnyi, 141701 Moscow region, Russia; e-mail: sedyakina.d@gmail.com

Received 14 July 2021
Kvantovaya Elektronika **51** (9) 826–832 (2021)
Translated by M.A. Monastyrskiy

regime of moderately nonlinear acceleration up to an energy of ~8 GeV, and also propose ways to minimise the emittance growth. The processes of smooth input and output of an electron bunch with the preservation of both emittance and depolarisation are investigated. The spin dynamics at a single separate stage is estimated using the Thomas–Bargmann–Michel–Telegdi (TBMT) equation [21] with no regard to the contribution of the Sokolov–Ternov effect, since the characteristic time of radiation polarisation resulting from the particle spin interaction with the radiation field for an electron with an energy of about several GeV turns out to be in wakefields several orders of magnitude longer than the time of particle interaction with the accelerating and focusing fields [18].

In examining the process of acceleration of a polarised electron to 4 TeV in model fields characteristic of various acceleration regimes, the spin dynamics was studied with allowance for the radiation friction force and the contribution of radiation polarisation using the semiclassical generalised TBMT equation [19, 20], which includes additives due to spin interaction of an electron with the field of the emitted photon.

2. Emittance dynamics in the wakefield

An electron bunch accelerated in the wakefield of a laser pulse moves under the action of a focusing force F_r and an accelerating force F_z, which are determined by the wakefield potential ϕ as [22]

$$F_r = E_r - B_\phi = \frac{\partial \phi}{\partial \rho}, \quad F_z = E_z = \frac{\partial \phi}{\partial \xi} \tag{2}$$

in dimensionless variables

$$\rho = k_\mathrm{p} r, \quad \xi = k_\mathrm{p}(z - ct), \tag{3}$$

where ϕ is normalised to mc^2/e; E_r, E_z, and B_ϕ are the electric and magnetic components of the wakefield, normalised to $mc\omega_\mathrm{p}/e$; e is the electron charge; c is the speed of light; m is the electron mass; ω_p is the plasma frequency; and $k_\mathrm{p} = \omega_\mathrm{p}/c$. The equations of motion for a relativistic electron can be written in the form

$$\frac{\mathrm{d}\boldsymbol{u}}{\mathrm{d}\zeta} = \frac{1}{\beta_z}(\nabla\phi + \boldsymbol{F}_\mathrm{rad}),$$

$$\frac{\mathrm{d}\xi}{\mathrm{d}\zeta} = 1 - \frac{1}{\beta_z}, \quad \frac{\mathrm{d}x}{\mathrm{d}\zeta} = \frac{u_x}{u_z}, \quad \frac{\mathrm{d}y}{\mathrm{d}\zeta} = \frac{u_y}{u_z}, \tag{4}$$

where $\boldsymbol{F}_\mathrm{rad}$ is the radiation friction force [23]; $\boldsymbol{u} = \boldsymbol{p}/(mc)$ is the normalised momentum of a particle; $\zeta = k_\mathrm{p} z$; x, y are the coordinates in the transverse plane; $\beta_z = u_z/\gamma$ is the dimensionless velocity component; and $\gamma = \sqrt{1 + u^2}$ is the particle gamma factor.

Let us consider the dynamics of the characteristics of a bunch of particles in a moderately nonlinear regime of laser-plasma acceleration. In the quasi-static approximation, in the case of a 'wide' (compared to the length $1/k_\mathrm{p}$) laser pulse, the evolution of the generated wakefield can be described by the expression [22]

$$\left[(\Delta_{\perp\rho} - v_0)\frac{\partial^2}{\partial\xi^2} - \frac{\partial \ln v_0}{\partial\rho}\frac{\partial^3}{\partial\rho\partial\xi^2} + v_0\Delta_{\perp\rho}\right]\phi - \frac{v_0^2}{2}\left[1 - \frac{1 + |a|^2/2}{(1+\phi)^2}\right] = v_0\Delta_{\perp\rho}\frac{|a|^2}{4}, \tag{5}$$

where $v_0 = n_0(\rho,\zeta)/n_{\mathrm{e}0}$; n_0 is the initial distribution of the electron density in the plasma channel; and $n_{\mathrm{e}0}$ is the initial density of electrons on the channel axis. The propagation of laser radiation with allowance for cylindrical symmetry was described by Maxwell's equations for the dimensionless complex envelope of the laser pulse $a(\rho, \xi, \zeta) = eE_\mathrm{las}/(mc\omega_0)$ [22], where ω_0 is the laser pulse frequency. In our work, the acceleration of electron bunches is considered in the field of a wake wave generated by an intense laser pulse in a plasma channel with a parabolic radial profile of the plasma concentration [24]:

$$n_\mathrm{e} = n_{\mathrm{e}0}\left[1 + \left(\frac{r}{R_\mathrm{ch}}\right)^2\right], \tag{6}$$

where R_ch is the channel radius. For simulation, we set the electron density on the plasma channel axis as $n_{\mathrm{e}0} = 10^{17}$ cm^{-3}, which corresponds to $k_\mathrm{p} = 0.0595$ μm^{-1}, the gamma factor of the wake wave phase velocity $\gamma_\mathrm{ph} = 132$, and the dephasing length in the linear limit $L_\mathrm{ph} = \lambda_0\gamma_\mathrm{ph}^3 \approx 180$ cm.

The laser pulse at the channel entrance had a Gaussian profile with the following parameters:

$$a_0 = 1.4, \quad t_0\omega_\mathrm{p} = 1, \quad r_0 k_\mathrm{p} = 5.3 \tag{7}$$

(a_0 is the normalised vector potential), which corresponds to the pulse duration $t_0 = 56$ fs, the focal spot radius $r_0 = 89$ μm, the intensity $I_0 \approx 4\times10^{18}$ W cm^{-2}, and the peak power $P \approx 530$ TW [$P_\mathrm{cr} \approx 0.0174\ \mathrm{TW}(\omega_0/\omega_\mathrm{p})^2 \approx 303$ TW] at a wavelength $\lambda_0 = 0.8$ μm. For partial compensation of relativistic and ponderomotive nonlinearities, the laser pulse duration was chosen to be shorter than the resonance duration $t_\mathrm{r} \approx \pi/\omega_\mathrm{p}$ [25]. Given the self-focusing processes, the plasma channel radius was chosen slightly larger than the matched (in a linear approximation) radius $R_\mathrm{ch} = 236.34$ μm and amounted to 305.1 μm [26].

The selected parameters of the laser pulse and plasma can be used to study the acceleration process at a separate accelerating stage of the laser-plasma collider, at which the maximum energy gain will be ~10 GeV at an acceleration length of 90 cm for electrons and ~5 GeV at a length of 50 cm for positrons [27].

Let us consider the acceleration of monoenergetic infinitely short electron bunches with an initial energy of $E_\mathrm{inj} = 67.5$ MeV in the absence of a radiation friction force, since at energies of the order of 10 GeV, its effect on the bunch acceleration process is small [14, 15]. All particles were injected into the vicinity of the accelerating force maximum with the same longitudinal coordinate ξ and had a Gaussian transverse distribution with different characteristic radii and momenta. In one case, all bunches had the same initial radius $r_\mathrm{b} = r_\mathrm{i} = 2.1$ μm ($r_\mathrm{b}k_\mathrm{p} = 0.125$) and different initial emittances: $\varepsilon_{xn}^{(0)} = 0.1$, 0.34, and 0.82 mm mrad, where $\varepsilon_{xn}^{(0)} = \varepsilon_{yn}^{(0)} = \varepsilon_\mathrm{n}^{(0)}/2$, and in the other case, the same initial emittance $\varepsilon_{xn}^{(0)} = 0.34$ mm mrad and different initial radii: $r_\mathrm{i} = 1$, 2.1, and 4.2 μm. The parameters $\varepsilon_{xn}^{(0)} = 0.34$ mm mrad and $r_\mathrm{i} = r_\mathrm{bm} = 2.1$ μm are matched in terms of the focusing force at the injection point [28, 29], which leads to an almost complete absence of bunch radius oscillations caused by betatron oscillations of particles. The modulating slow (with respect to

betatron) radius oscillations are stipulated by the nonlinear dynamics of the laser pulse in the channel and, as a result, the nonstationarity of the focusing [$F_r = \alpha(\rho,\xi,\zeta)\rho$] and accelerating [$F_z = F_z(\rho,\xi,\zeta)$] forces (Figs 1 and 2). In this case, the root-mean-square radius decreases with increasing energy, and its change, with the known dynamics of the dimensionless betatron frequency Ω, can be described by the expression [29]

$$r_b = r_i\left[\frac{\gamma_0\Omega_0}{\gamma(\zeta)\Omega(\zeta)}\right]^{1/2}, \qquad (8)$$

where Ω_0 and γ_0 are the initial values of the betatron frequency and the gamma factor of electrons.

In other mismatched cases, the radius will oscillate in the range of values determined by r_i and $r_{bm}^2/r_i[r_{bm}^2 = \varepsilon_n^{(0)}k_p/(\gamma_0\Omega_0)]$ [28] (Figs 1 and 2), while the lower and upper envelopes of these oscillations will change according to (8) with the corresponding r_i (r_i or r_{bm}^2/r_i). In Fig. 2, dashed lines show the dynamics (8) of the matched bunch radius with $\varepsilon_{xn}^{(0)}$ = 0.3 mm mrad and r_i = 2.1 μm, as well as the dynamics of the envelopes of mismatched bunches with the same emittance, but with r_i = 1 or 4.2 μm. The dynamics of Ω for (8) was taken at a distance of $0.1/k_p$ from the axis from the results of self-consistent simulation with the parameters described above.

The emittance of an infinitely short electron bunch with an adiabatic change in the accelerating and focusing fields in a linear focusing force and an accelerating force constant along the radius should be preserved both in the matched and mismatched cases [30]. However, as shown in Figs 3 and 4, an increase in this emittance is observed in almost all mismatched cases, which means mixing of the oscillation phases of the bunch electrons and violation of one or several of the conditions specified above.

Figure 5 shows the emittance dynamics of an infinitely short electron bunch with initial parameters $\varepsilon_{xn}^{(0)}$ = 0.82 mm mrad and r_b = 2.1 μm in different model fields and in self-consistent simulation. The blue curve corresponds to the case of bunch acceleration under the action of a homogeneous constant accelerating force and a linear focusing force, the characteristic values of which were found by averaging the

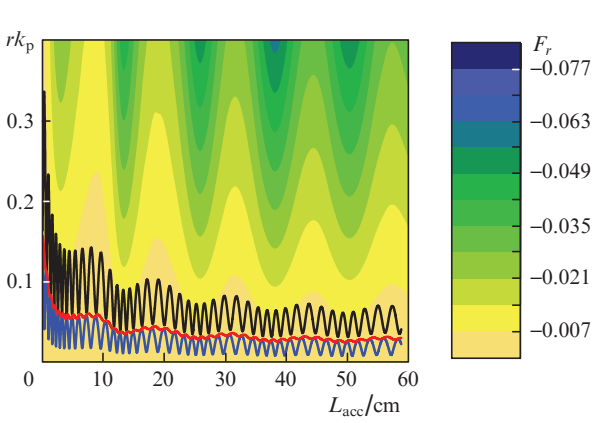

Figure 1. (Colour online) Dependences of the average radius of electron bunches with an initial radius r_b = 2.1 μm and energy E_{inj} = 67.5 MeV on the acceleration length (curves), as well as the two-dimensional distribution of the focusing force (colour scale). The blue curve corresponds to the case of bunch acceleration with a mismatched initial emittance $\varepsilon_{xn}^{(0)}$ = 0.1 mm mrad; the red curve, with a matched initial emittance $\varepsilon_{xn}^{(0)}$ = 0.34 mm mrad; and the black curve, with a mismatched initial emittance $\varepsilon_{xn}^{(0)}$ = 0.82 mm mrad.

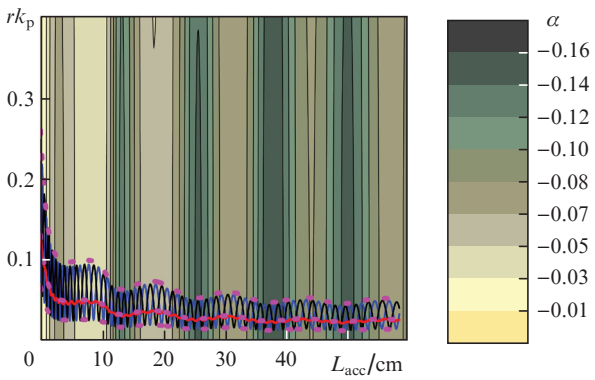

Figure 2. (Colour online) Dependences of the average radius of electron bunches with an initial emittance $\varepsilon_{xn}^{(0)}$ = 0.34 mm mrad and energy E_{inj} = 67.5 MeV on the acceleration length (curves), as well as the two-dimensional distribution of the focusing force parameter α (colour scale). The blue curve corresponds to the case of acceleration of a bunch with a mismatched initial radius r_b = 1 μm; the red curve, with a matched initial radius r_b = 2.1 μm; the black curve, with a mismatched initial radius r_b = 4.2 μm; and the pink dashed curves are the values obtained according to formula (8) for r_i = 1, 2.1, and 4.2 μm.

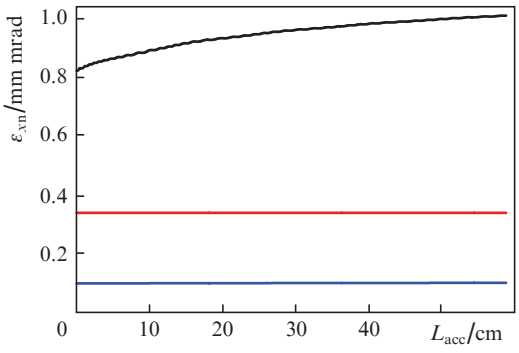

Figure 3. (Colour online) Dependences of the emittance ε_{xn} of electron bunches with an initial radius r_b = 2.1 μm and energy E_{inj} = 67.5 MeV on the acceleration length. The blue curve corresponds to the case of bunch acceleration with a mismatched initial emittance $\varepsilon_{xn}^{(0)}$ = 0.1 mm mrad; the red curve, with a matched initial emittance $\varepsilon_{xn}^{(0)}$ = 0.34 mm mrad; and the black curve, with a mismatched initial emittance $\varepsilon_{xn}^{(0)}$ = 0.82 mm mrad.

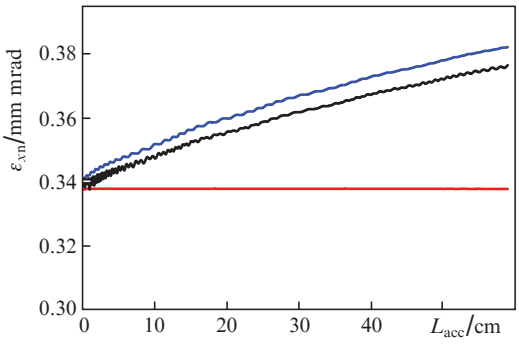

Figure 4. (Colour online) Dependences of the emittance of electron bunches with an initial emittance $\varepsilon_{xn}^{(0)}$ = 0.34 mm mrad and energy E_{inj} = 67.5 MeV on the acceleration length. The blue curve corresponds to the case of acceleration of a bunch with a mismatched initial radius of r_b = 1 μm; the red curve, with a matched initial radius r_b = 2.1 μm; and the black curve, with a mismatched initial radius r_b = 4.2 μm.

forces acting on individual particles over the entire length of the wake acceleration. The red curve shows the emittance dynamics at a homogeneous constant accelerating force and a nonlinear constant focusing force, the values of which at different distances from the axis were taken at an acceleration length of $L_{acc} = 30$ cm. In the case described by the black curve, the focusing force dynamics is obtained from the simulation results for the above parameters, while the accelerating force is homogeneous and constant. The green curve shows the emittance dynamics in the calculated fields and corresponds to the black curve in Fig. 3.

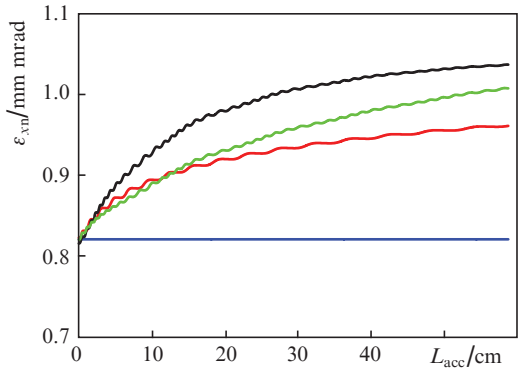

Figure 5. (Colour online) Dependences of the emittance of an electron bunch with an initial radius $r_b = 2.1$ μm, energy $E_{inj} = 67.5$ MeV, and a mismatched initial emittance $\varepsilon_{xn}^{(0)} = 0.82$ mm mrad on the acceleration length at various focusing and accelerating forces. The blue curve corresponds to a linear stationary focusing force and a homogeneous constant accelerating force; the red curve, to a stationary nonlinear focusing force and a homogeneous constant accelerating force; the black curve, to a nonstationary nonlinear focusing force and a homogeneous constant accelerating force; and the green curve is the result of self-consistent simulation (all forces are nonstationary and nonlinear in radius).

It can be seen from Fig. 5 that the greatest contribution to the emittance growth at given parameters is made by the nonlinearity of the focusing force along the radius, and the mechanism of mixing of electron phases in the bunch slice is mainly explained by the difference in the values of the coefficient $\alpha = \alpha(\rho, \xi, \zeta)$ of the focusing force for particles located at different distances from the axis. To minimise the effect of this process on the emittance growth, it is necessary to inject a bunch into the axis vicinity with parameters that ensure a small change in α during the acceleration process with oscillations of the root-mean-square radius of the bunch between $r_b(r_i, \zeta)$ and $r_b(r_{bm}^2/r_i, \zeta)$ (for example, the matched and mismatched cases at $\varepsilon_{xn}^{(0)} = 0.1$ mm mrad and $r_b = 2.1$ μm in Figs 1 and 3).

3. Input of polarised electrons into the accelerating stage and their output from it

The scheme of a multistage accelerator assumes multiple input of electron bunches into the plasma channel and their output from it, as well as the transportation of these bunches between accelerating cascades. We examine the processes of input and output of electrons while maintaining their initial polarisation. Studies [10, 11] show that in order to ensure adiabatic changes in the forces and minimise the bunch emittance growth at each stage, the characteristic time of the field change at the input and output should be several times greater than the period $\lambda_\beta/c = 1/(\Omega k_p)$ of betatron oscillations of particles in the bunch.

Consider the acceleration of a bunch of polarised electrons in a parabolic plasma channel with a smooth input of length $\sim 3\lambda_\beta$ and a smooth output of length $\sim 2\lambda_\beta$. The initial parameters of the laser pulse were set in such a way that the focal plane position during the laser pulse propagation in vacuum coincided with the onset of the homogeneous part of the channel, and the plasma concentration in this part of the channel and the pulse characteristics in the focal plane were chosen in accordance with the moderately nonlinear acceleration regime described in the previous section. The density $n_0(\rho, \zeta)$ of electrons in the plasma increased linearly at the input to $z = 5.77$ cm and decreased linearly at the output, starting from $z = 55.27$ cm. In this case, the channel radius decreased linearly from 398.5 μm at the input and increased at the output to 460.8 μm, taking a constant value of 305.1 μm in the range $5.27 \leqslant z \leqslant 55.27$ cm (Fig. 6a). The laser pulse dynamics in such a channel is shown in Fig. 6b.

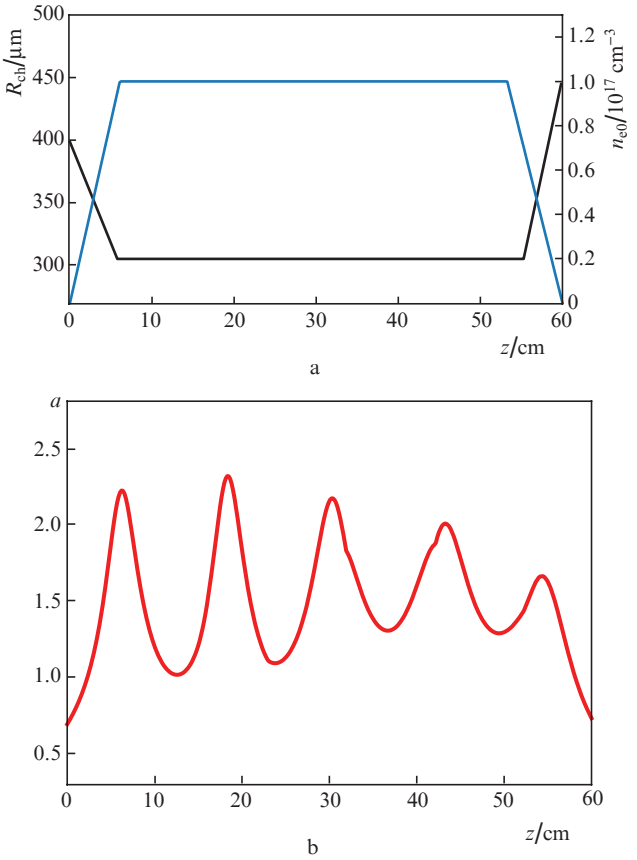

Figure 6. (Colour online) (a) Plasma channel radius (black curve) and the density of plasma electrons on the axis (blue curve), as well as (b) dynamics of the dimensionless amplitude a of the laser pulse during propagation in the channel with smooth input and output. The pulse is focused at point $z = 5.27$ cm, which coincides with the onset of the channel section with a constant radius. The desnity plateau begins at $z = 5.77$ cm.

The motion of individual particles of the bunch was described using the relativistic Lorentz equation (4) without taking into account the radiation friction force, while the dynamics of the spin $\boldsymbol{s}$ was described by the TBMT equation [21]

$$\frac{\mathrm{d}\boldsymbol{s}}{\mathrm{d}\tau} = \boldsymbol{s}\times(a_\mathrm{m}\boldsymbol{B}_\mathrm{R} + \boldsymbol{B}_E), \tag{9}$$

$$\boldsymbol{B}_E = \boldsymbol{B} + \frac{1}{1+1/\gamma}\boldsymbol{E}\times\boldsymbol{v}, \tag{10}$$

$$\boldsymbol{B}_\mathrm{R} = \gamma\left[\boldsymbol{B} - \frac{\boldsymbol{v}(\boldsymbol{v}\boldsymbol{B})}{1+1/\gamma} - \boldsymbol{v}\times\boldsymbol{E}\right], \tag{11}$$

where a_m is the anomalous magnetic moment of the electron; $\tau = t\omega_\mathrm{p}$; $\boldsymbol{v}$ is the particle velocity normalised to the speed of light; and $\boldsymbol{B}$ and $\boldsymbol{E}$ are the dimensionless magnetic and electric fields in the laboratory reference frame. Equations (4) and (9)–(11), in which the combination of fields $\boldsymbol{B} = (0, 0, B_\phi)$ and $\boldsymbol{E} = (E_z, E_r, 0)$ is reduced to the forces F_r and F_z [5, 31], represent together with Eqn (5) a closed self-consistent system of equations describing the acceleration of a polarised charged particle in the field of a wake wave generated by a laser pulse in the plasma channel [31].

The injected electron bunch had Gaussian longitudinal and transverse distributions of particles, with a characteristic initial radius of $r_\mathrm{b} = 3.5$ μm and a length of $z_\mathrm{b} = 0.5$ μm. The transverse emittance $\varepsilon_{xn}^{(0)} = \varepsilon_{yn}^{(0)} = 0.132$ mm mrad was chosen matched with the focusing force at point $z = 0.25$ cm. At the injection time moment, all particles had the same energy $E_\mathrm{inj} = 67.5$ MeV and the spin vector $\boldsymbol{s} = (0.279, -0.335, 0.9)$.

During a single accelerating stage, the particles gained ~8 GeV over a length of 60 cm (taking into account the input to the channel and output from it). The maximum absolute value of depolarisation and the bunch emittance were preserved during the acceleration and extraction of electrons from the channel, but increased at the initial stages of acceleration, which, however, did not affect the final value of depolarisation (Fig. 7). The polarisation vector $\boldsymbol{P}$ of a bunch of particles meant a vector averaged over the spins of all particles, and the bunch's depolarisation value $-|\Delta\boldsymbol{P}|$ was equal to the modulus of the difference between the initial ($\boldsymbol{P}_0$) and current ($\boldsymbol{P}$) polarisation vectors taken with the opposite sign ($-|\boldsymbol{P} - \boldsymbol{P}_0|$).

A jump-like increase in the bunch emittance and depolarisation oscillations with large amplitudes at the initial stages of acceleration mean that a more careful choice of the concentration profile at the channel input is required.

4. Radiation polarisation effect in a laser-plasma accelerator

The characteristic time of radiation polarisation (1) can be represented in dimensionless form:

$$\frac{1}{T} = \frac{5\sqrt{3}}{8}\frac{\tilde{\alpha}\hbar^2 k_\mathrm{p}^2}{m^2c^2}\gamma^5|\dot{\boldsymbol{v}}|^3, \tag{12}$$

where $\tilde{\alpha}$ is the fine structure constant, and $\dot{\boldsymbol{v}} = \mathrm{d}\boldsymbol{v}/\mathrm{d}t$.

The probability of a quantum transition of an electron with a change in the spin projection during photon emission

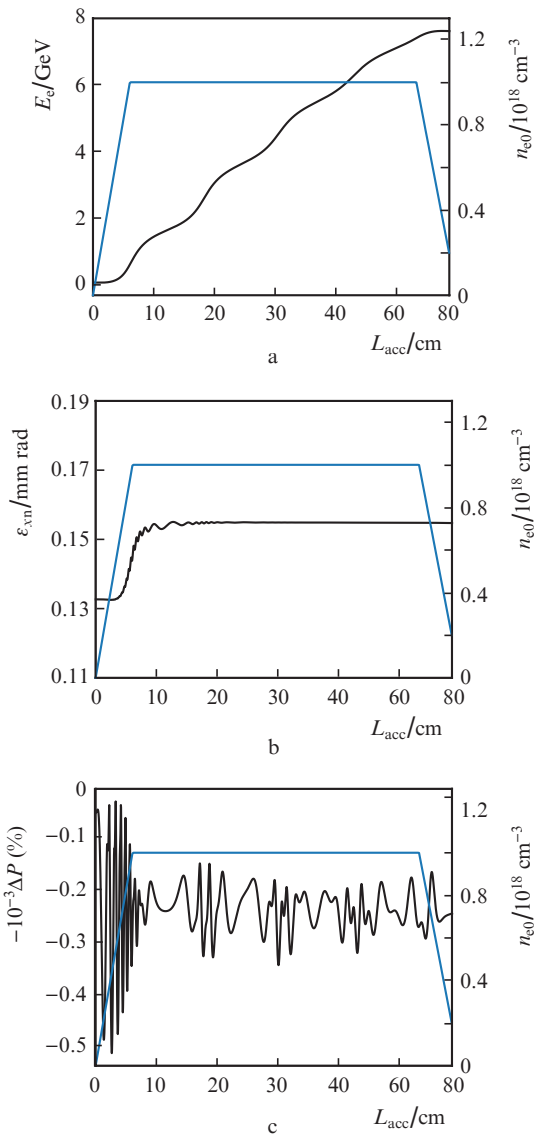

Figure 7. (Colour online) Dynamics of (a) energy gain, (b) emittance and (c) depolarisation during acceleration of an electron bunch with an initial energy $E_\mathrm{inj} = 67.5$ MeV, radius $r_\mathrm{b} = 3.5$ μm, length $z_\mathrm{b} = 0.5$ μm, and a transverse emittance $\varepsilon_{xn}^{(0)} = 0.132$ mm mrad (black curves). The blue curves correspond to the initial distribution of the plasma electron density on the channel axis.

can be described for an arbitrary magnetic field by the expression [19, 20]

$$W = \frac{1}{T}\left[1 - \frac{2}{9}(\boldsymbol{s}\boldsymbol{v})^2 + \frac{8\sqrt{3}}{15|\dot{\boldsymbol{v}}|}(\boldsymbol{s}, \boldsymbol{v}\times\dot{\boldsymbol{v}})\right] \tag{13}$$

provided that $\gamma \gg 1$ and the field varies slightly along the particle trajectory during the characteristic radiation time t_rad [20]:

$$\frac{|\dot{\boldsymbol{B}}|t_\mathrm{rad}}{|\boldsymbol{B}|} \ll 1, \quad |\dot{\boldsymbol{v}}|t_\mathrm{rad} \approx \frac{1}{\gamma}. \tag{14}$$

Then the dynamics of the vector $\boldsymbol{s}$ under the action of synchrotron radiation, given the precession (9)–(11) and equations (2) and (4), takes the form [19, 20]:

$$\frac{\mathrm{d}\boldsymbol{s}}{\mathrm{d}\tau} = \boldsymbol{s}\times(a\boldsymbol{B}_{\mathrm{R}} + \boldsymbol{B}_{E})$$

$$-\frac{1}{T}\left[\boldsymbol{s} - \frac{2}{9}(\boldsymbol{s}\boldsymbol{v})\boldsymbol{s} + \frac{8}{5\sqrt{3}|\boldsymbol{F} - \boldsymbol{v}(\boldsymbol{F}\boldsymbol{v})|}\boldsymbol{v}\times\boldsymbol{F}\right], \qquad (15)$$

where $\boldsymbol{F} = \nabla\phi + \boldsymbol{F}_{\mathrm{rad}}$ [14, 15, 23].

Let us now consider the acceleration of an electron to an energy of ~4 TeV in model fields characteristic of various regimes of laser-plasma acceleration, with a focusing force $F_r = \alpha\rho$ linear along the radius and a homogeneous constant accelerating force F_z, taking into account the radiation friction force in the Landau–Lifshitz form. At the initial time moment, the electron was at a distance of $0.5/k_{\mathrm{p}}$ from the axis (the characteristic distance from the axis to the electron in the bunch) with zero transverse momentum, spin $\boldsymbol{s}$ = (0.279, −0.335, 0.9), and energy E_{inj} = 67.5 MeV.

In the first case, we set $\alpha = -0.5$ and $F_z = 2$, which corresponds to the particle motion in the maximum of the accelerating field generated in the bubble regime as a result of the laser pulse interaction at the parameters $a_0 = 4$, intensity $I_0 \approx 3.5\times10^{19}$ W cm^{-2}, peak power $P \approx 2.5$ PW, spot size $r_0 = 67$ μm, and radiation wavelength $\lambda_0 = 0.8$ μm, with plasma having the density $n_{\mathrm{e}} = 10^{17}$ cm^{-3} [32]. In this case, the accelerating field's gradient was 60 GeV m^{-1}, and the characteristic self-polarisation time (1) was ~0.5 ns for an electron with an energy of ~1 TeV. The time of particle acceleration to an energy of ~4 TeV in the absence of the radiation friction force was about 0.2 μs, and, with allowance for synchrotron radiation, about 0.7 μs (Fig. 8a). It can be seen from Fig. 8b that, despite the smallness of the characteristic self-polarisation time compared to the particle acceleration time, the contribution of radiation polarisation at the given parameters only leads to a slight decrease in the upper boundary of the depolarisation envelope, and the greatest effect is exerted by the radiation friction force, which causes a decrease in the absolute value of the final depolarisation by about 1.5 times. The correction to the TBMT equation leads to a slight damping of the oscillations of the longitudinal spin component s_z, starting from energies of ~2 TeV (Fig. 8c).

In the regime of moderately nonlinear acceleration described in the previous sections, the average accelerating and focusing forces are several times weaker than the forces acting on a particle in the bubble regime. The characteristic focusing force has a coefficient $\alpha \approx -0.075$, the accelerating force is $F_z \approx 0.47$, and the accelerating field gradient is 14 GeV m^{-1}. The corresponding self-polarisation time in such fields for an electron with an energy of 1 TeV is about 36 ns, and the acceleration time to 4 TeV is about 1 μs (Fig. 9, a). However, according to the simulation results, the effect of radiation polarisation in this case turns out to be negligibly small, while the radiation friction force slightly reduces the amount of depolarisation, starting with an energy of 2 TeV (Fig. 9).

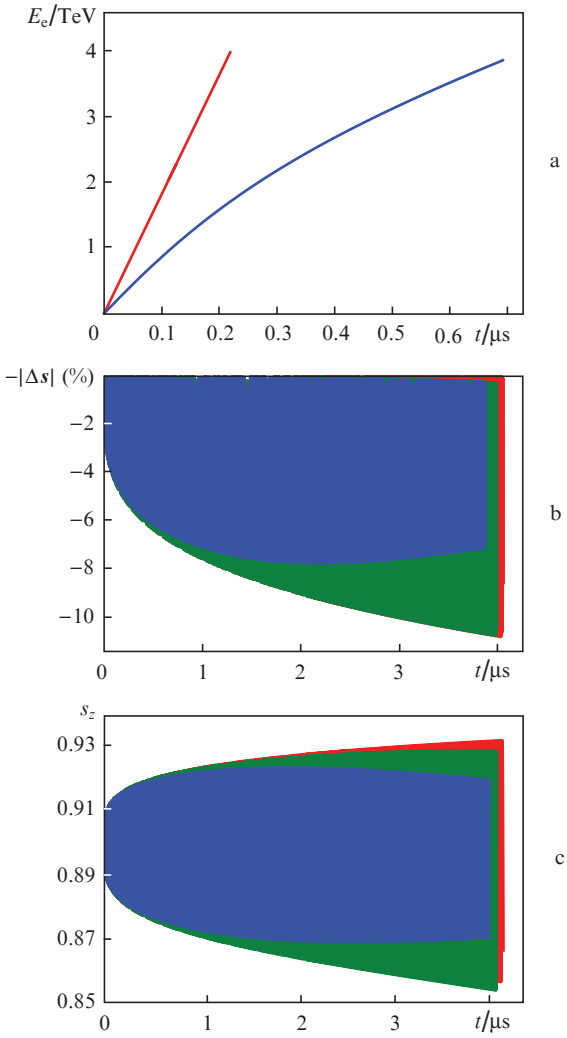

Figure 8. (Colour online) Dynamics of the characteristics of an electron with an initial energy E_{inj} = 67.5 MeV and a longitudinal spin component s_z = 0.9, injected at a distance of $0.5/k_{\mathrm{p}}$ from the axis with zero transverse momentum in the model bubble-acceleration regime. The blue curves correspond to the energy gain depending on (a) acceleration time, (b) particle depolarisation, and (c) dynamics of the spin component s_z depending on the accumulated energy with regard to the radiation friction force and the radiation polarisation effect. The green curves correspond to (b) particle depolarisation and (c) dynamics of the spin component s_z depending on the accumulated energy with regard to the radiation polarisation effect and disregarding the radiation friction force. The red curves correspond to the energy gain depending on (a) acceleration time, (b) particle depolarisation, and (c) dynamics of the spin component s_z depending on the accumulated energy disregarding the effects associated with synchrotron radiation.

5. Conclusions

We have considered a number of issues related to the preservation of the quality of polarised electron bunches in a multistage laser-plasma accelerator. The mechanism of emittance growth for an infinitely short bunch in a moderately nonlinear acceleration regime suitable for use at a separate stage of a multi-stage accelerator is determined. It is shown that the greatest contribution to the emittance growth is made by the process of mixing the phases of betatron oscillations of individual particles of the bunch due to the nonlinear dependence of the focusing force on the radius. To prevent phase mixing in the bunch slice, it is necessary to minimise the change in the focusing force parameter α on a scale of the order of the amplitude of betatron oscillations of particles in the bunch by injecting the bunch into a small vicinity of the laser bunch axis with parameters that provide particle oscillations in the region of the focusing force linearity.

In order to inject a bunch of particles into the accelerating stage and remove it from there after acceleration for subsequent transportation with the preservation of the initial char-

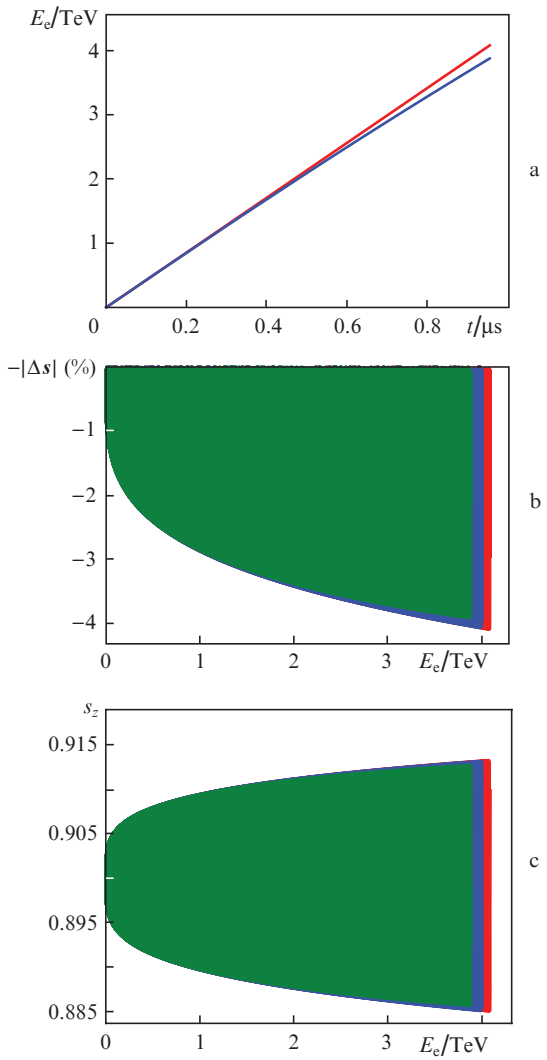

Figure 9. (Colour online) Same as in Fig. 8, but in a model moderately nonlinear acceleration regime.

acteristics, it is necessary to ensure an adiabatic change in wakefields during the period of betatron oscillations at the input and output of the plasma channel. In this work, we have considered the acceleration of polarised electrons in a channel with a linear increase in the density of electrons on the channel axis and a simultaneous decrease in its radius at the entrance to the accelerating stage, and with a linear decrease in the density and a simultaneous increase in the channel radius at the exit from this stage. With the parameters used, the maximum absolute value of polarisation is preserved during the acceleration and extraction of the bunch, experiencing oscillations at the time moment the bunch enters the stage. The bunch emittance increases abruptly at the initial stages of acceleration and preserves in the process of extracting particles from the channel, which means that a more careful selection of the density profile at the channel input is required.

With further acceleration of electrons to energies of several TeV, the effect of synchrotron radiation of particles on the dynamics of the bunch characteristics becomes significant. We have considered the acceleration of polarised particles in model fields characteristic of the moderately nonlinear regime and the bubble regime of laser-plasma acceleration taking into account the radiation friction force in the Landau–Lifshitz form, while the polarisation dynamics has been estimated using the generalised TBMT equation with regard to the contribution of radiation polarisation. As the results of calculations show, despite the fact that the calculated characteristic time of radiation polarisation for electrons with energies about 1 TeV in wakefields is several orders of magnitude shorter than the time of particle acceleration, the total contribution of this effect to the depolarisation process turns out to be insignificant for both regimes under study, while the radiation friction force leads to a significant decrease in depolarisation in strong focusing fields corresponding to the bubble acceleration regime.

Acknowledgements. The reported study was funded by RFBR, project number 19-02-00908-A, and RFBR and ROSATOM, project number 20-21-00150.

References

1. Gonsalves A.J. et al. *Phys. Rev. Lett.*, **122**, 084801 (2019).
2. Leemans W.P. et al. *Phys. Rev. Lett.*, **113**, 245002 (2014).
3. Nakajima K. *Nucl. Instrum. Methods Phys. Res. Sect. A*, **455**, 140 (2000).
4. Malka V. et al. *Science,* **298**, 1596 (2002).
5. Vieira J. et al. *Phys. Rev. Spec. Top. Accel. Beams*, **14**, 071303 (2011).
6. Leemans W., Esarey E. *Phys. Today*, **62**, 44 (2009).
7. Walker P.A. et al. *J. Phys. Conf. Ser.*, **874**, 012029 (2020).
8. Weikum M.K. et al. *AIP Conf. Proc.*, **2160**, 040012 (2019).
9. Assmann R.W. et al. *Eur. Phys. J. Spec. Top.*, **229**, 3675 (2020).
10. Tomassini P., Rossi A. *Plasma Phys. Controlled Fusion*, **58**, 034001 (2015).
11. Li X., Chancé A., Nghiem P.A.P. *Phys. Rev. Accel. Beams*, **22**, 021304 (2019).
12. Mane S., Shatunov Y.M., Yokoya K. *Rep. Prog. Phys.*, **68**, 1997 (2005).
13. Moortgat-Pick G. et al. *Phys. Rep.*, **460**, 131 (2008).
14. Kostyukov I.Y., Nerush E., Litvak A. *Phys. Rev. Spec. Top. Accel. Beams*, **15**, 111001 (2012).
15. Pugacheva D.V., Andreev N.E. *Quantum Electron.*, **48**, 291 (2018) [*Kvantovaya Elektron.*, **48**, 291 (2018)].
16. Michel P. et al. *Phys. Rev. E*, **74**, 026501 (2006).
17. Sokolov A.A., Ternov I.M. *Dokl. Akad. Nauk SSSR*, **153**, 1052 (1963).
18. Thomas J. et al. *Phys. Rev. Accel. Beams*, **23**, 064401 (2020).
19. Ternov I.M. *Fiz. Elem. Chast. Atom. Yadra*, **17**, 884 (1986).
20. Baier V.N. *Sov. Phys. Usp.*, **14**, 695 (1972) [*Usp. Fiz. Nauk*, **105**, 441 (1971)].
21. Bargmann V., Michel L. Telegdi V.L. *Phys. Rev. Lett.*, **2**, 435 (1959).
22. Andreev N.E., Nishida Y., Yugami N. *Phys. Rev. E*, **65**, 056407 (2002).
23. Landau L.D., Lifshits E.M. *The Classical Theory of Fields* (London: Butterworth-Heinemann, 1975; Moscow: Nauka, 1988).
24. Andreev N.E., Kirsanov V.I., Gorbunov L.M. *Phys. Plasmas*, **2**, 2573 (1995).
25. Andreev N.E., Kuznetsov S.V. *Plasma Phys. Controlled Fusion*, **45**, A39 (2003).
26. Andreev N.E. et al. *Phys. Plasmas*, **4**, 1145 (1997).
27. Pugacheva D.V., Andreev N.E. *Vestnik OIVT RAN*, **5**, 13 (2020).
28. Esarey E. et al. *Phys. Rev. E*, **65**, 056505 (2002).
29. Veisman M.Ye., Andreev N.E. *Quantum Electron.*, **50**, 392 (2020) [*Kvantovaya Elektron.*, **50**, 392 (2020)].
30. Reiser M., O'Shea P. *Theory and Design of Charged Particle Beams* (Wiley, 1994) Vol. 312.
31. Pugacheva D.V., Andreev N.E. *Quantum Electron.*, **46**, 88 (2016) [*Kvantovaya Elektron.*, **46**, 88 (2016)].
32. Esarey E., Schroeder C., Leemans W. *Rev. Mod. Phys.*, **81**, 1229 (2009).